ACS APPLIED MATERIALS & INTERFACES

Research Article

www.acsami.org

Template-Free Synthesis of a Porous Organic–inorganic Hybrid Tin(IV) Phosphonate and Its High Catalytic Activity for Esterification of Free Fatty Acids

Arghya Dutta,[†] Astam K. Patra,[†] Hiroshi Uyama,[‡] and Asim Bhaumik*[,†]

[†]Department of Materials Science, Indian Association for the Cultivation of Science, Jadavpur, Kolkata 700032, India

[‡]Department of Applied Chemistry, Graduate School of Engineering, Osaka University, 2-1 Yamadaoka, Suita, Osaka 565-0871, Japan

Supporting Information

ABSTRACT: Here we have synthesized an organic–inorganic hybrid mesoporous tin phosphonate monolith (MLSnP-1) with crystalline pore walls by a template-free sol–gel route. N_2 sorption analysis shows Brunauer–Emmett–Teller (BET) surface area of 347 m^2g^{-1}. Wide-angle powder X-ray diffraction (PXRD) pattern shows few broad diffraction peaks indicating crystalline pore wall of the material. High-resolution transmission electron microscopic (HR TEM) image further reveals the crystal fringes on the pore wall. Framework bonding and local environment around phosphorus and carbon were examined by Fourier transform infrared (FT IR) spectroscopy and solid-state MAS NMR spectroscopy. The material exhibits remarkable catalytic activity for esterification of long chain fatty acids under mild reaction conditions at room temperature.

KEYWORDS: *catalysis, esterification reaction, hybrid material, mesoporous material, porous monolith, tin phosphonate*

INTRODUCTION

Organic–inorganic hybrid porous solids are an important class of materials because of their wide scale potentials in many emerging fields, such as catalysis,[1] drug delivery,[2] optoelectronics,[3,4] gas storage,[5] etc. These hybrid materials merge the rigidity of inorganic solids with versatile functionality of organic building blocks that can be incorporated under very soft and sustainable synthesis conditions. As a subclass of hybrid porous solids, metal phosphonates draw huge interests because of their application in catalysis,[6] gas storage,[7] ion adsorption,[8] etc. Synthesis procedures of these materials involve both templated and nontemplated routes and most of these materials are powdery solids. Between these two routes, nontemplated pathway is generally preferred because removal of template sometimes leads to collapse of pore structure. On the other side, if the porous materials have monolithic structure they exhibit several advantages over powdery porous materials. Porous monoliths find extensive applications in chromatography,[9] separation science,[10] and catalysis.[11] To date, maximum efforts have been paid to the development of hybrid silica[12] and polymer-based[13]monolithic porous materials. But despite multifarious applications of transition metal chemistry,[14] there are many fewer reports on transition-metal-based porous monoliths. There are few reports on monolithic porous metal oxides,[15,16] but other types are rarely explored in this regard.[17] However, monolithic nature of designed metal phosphonates under template-free synthesis route is unprecedented. The main target of this area of research was to synthesize porous monoliths with hierarchical porosity, and pore walls of these materials were mostly amorphous. But amorphous pore wall often limits the utility of a porous material for some practical applications.[18] Heat treatment for crystallization of pore wall is not always successful and can lead to collapse of the pore structure. Few metal oxide monoliths showed crystalline pore walls but surface area of these materials was very low.[11,19] Here we report a template free direct sol–gel synthesis of a mesoporous hybrid tin(IV) phosphonate monolith with high surface area and crystalline pore wall. Previously reported tin phosphonate materials are mostly microporous and these materials show either amorphous or layered structure.[20−22] These porous tin phosphonates are known to be efficient catalysts for different oxidation reactions. Earlier reports show that tin containing materials also act as solid acid catalysts for esterification and transesterification reactions for biodiesel synthesis.[23] This particular topic of research is also of enormous importance because scarcity of hydrocarbon reserve and growing environmental pollution due to emission of greenhouse gases have enhanced the demand for renewable energy sources. In this regard, biodiesel is an attractive alternative to reduce the consumption of fossil fuels. Biodiesels are renewable, biodegradable, and less polluting and can be synthesized by transesterification of triglycerides or esterification of free fatty acids (FFAs). Industrial production of esters and transesterification reactions involve use of homogeneous acid and alkaline catalysts which are of serious environmental concern and pose difficulties in separation and purification of

Received: April 26, 2013
Accepted: September 17, 2013
Published: September 17, 2013

the products. In addition, homogeneous alkaline catalysts are not compatible with FFAs. Esterification of FFAs before transesterification of triglycerides seems to be a solution to this problem. So our interest was to verify the acid catalytic activities of MLSnP-1 for the esterification of FFAs. Different commercially available long chain fatty acids were selected as representatives of FFAs to test the feasibility of the reaction. This material was found to be very efficient at mild reaction conditions including room-temperature synthesis.

EXPERIMENTAL SECTION

Materials. Phytic acid (50% in water; M_r = 660.04) or (1*R*,2*R*,3*S*,4*S*,5*R*,6*S*)-cyclohexane-1,2,3,4,5,6-hexayl hexakis-[dihydrogen (phosphate)] was purchased from Sigma Aldrich. Tin(IV) chloride pentahydrate ($SnCl_4{\cdot}5H_2O$; M_r = 350.58) and fatty acids were obtained from Loba Chemie. Methanol and ethanol were purchased from Merck. All the reagents were used without further purification. Unless otherwise stated, double distilled water was used in all the cases.

Material Synthesis. Phytic acid (4.4 g, 3.3 mmol) was dissolved in 20 g of water−ethanol (1:1 w/w) mixed solvent and was stirred for 30 min. To this solution was added 3.5 g of $SnCl_4{\cdot}5H_2O$ (10.0 mmol) dissolved in 5 g of H_2O. Gel formation started within 2 min after the addition of tin(IV) chloride solution and complete phase separation was observed within 5 min. Finally, the gel formed a monolithic structure. To prepare monoliths with defined shapes, we transferred the initial sol to glass vials before gelation and monoliths were allowed to form inside the vials. These as-synthesized monoliths were hydrothermally treated at 373 K for 72 h by immersing the glass vials in water inside a polypropylene bottle. Finally, the monoliths were very carefully dried slowly at room temperature.

Catalysis. In a typical catalytic process, 1 mmol of a fatty acid was dissolved in 5 mL of methanol (which could act both as reactant and solvent) and 30 mg of the MLSnP-1 catalyst (coarse chunks of up to 1 mm in diameter) was added. The catalytic reactions were carried out at 298 and 323 K in a round-bottom flask under stirring. Progress of the reaction was monitored by analysis of the reaction mixture by TLC at different time interval and the reactions were continued up to desired times as required for different substrates. After completion of the reaction, the reaction mixture was filtered to separate the catalyst and the filtrate was evaporated in a rotary evaporator to get the product. In the final product, no trace of excess unreacted acid was detected (checked by TLC) and it indicates complete conversion of the fatty acids. Final reaction products were characterized by ^{1}H and ^{13}C NMR spectra. Finally yield was calculated from purified products.

When equal amount (w/w) of fatty acids and methanol was used, after the required time, chloroform was added to the reaction mixture and the catalyst was filtered. The organic layer in the filtrate was repeatedly washed with 2% sodium bicarbonate solution to remove excess fatty acid. The organic layer was evaporated to obtain the final product.

Transesterification reaction of 1 mmol ethyl cyanoacetate was also carried out at 323 K in 5 mL methanol using 30 mg MLSnP-1 catalyst.

Catalyst Recycling Efficiency. To check the recycling efficiency, the catalyst was used for 5 consecutive cycles for esterification of lauric acid at 323 K and in each cycle the filtered catalyst was washed repeatedly by water−ethanol mixture and dried at room temperature.

Leaching Test. The true heterogeneity of the catalyst was verified by leaching test. In a typical esterification reaction of lauric acid with methanol at 323 K the catalyst was filtered after 2 h and the reaction was continued for 6 h. Amount of tin present in the solution was also tested by atomic absorption spectrophotometer (AAS).

Characterization. Elemental analyses were carried out by using a Shimadzu AA-6300 atomic absorption spectrophotometer (AAS) fitted with a double beam monochromator and Perkin-Elmer 2400 Series-II CHN analyzer. Thermogravimetry (TG) and differential thermal analyses (DTA) of the sample was carried out between the temperature ranges 298 to 1073 K in a TA Instruments thermal analyzer TA-SDT Q-600. Fourier transform infrared (FT IR) spectrum of the material was recorded using a Nicolet MAGNA-FT IR 750 Spectrometer Series II. Solid-state MAS NMR studies have been performed by using Chemagnetics 300 MHz CMX 300 spectrometer. Powder X-ray diffraction (PXRD) patterns were recorded on a Bruker D-8 Advance diffractometer operated at 40 kV and 40 mA and calibrated with a standard silicon sample, using Ni-filtered Cu Kα (λ = 0.15406 nm) radiation. Nitrogen adsorption/desorption isotherms were obtained by using a Beckman Coulter SA 3100 Surface Area Analyzer at 77 K. JEOL JEM 6700F field emission scanning electron microscope (SEM) was used for the determination of morphology of powder samples. The pore structure was explained by a JEOL JEM 2010F transmission electron microscope (TEM) operated at an accelerating voltage of 200 kV. ^{1}H and ^{13}C NMR experiments were carried out on Bruker DPX-300/500 NMR Spectrometer.

RESULTS AND DISCUSSION

Mesophase and Materials Characterization. MLSnP-1 was synthesized by using phytic acid (see Scheme S1 in the Supporting Information) as the phosphonate source and $SnCl_4{\cdot}5H_2O$ as the inorganic precursor. Previous studies show that multidentate organophosphonic acid ligands are able to form framework porosity with crystalline pore walls under hydrothermal condition without using any structure directing agent.[6,8,24] It reduces one extra step of template removal and avoids the associated possible problem of structure collapse. But those materials were polycrystalline powder and no monolithic metal phosphonate with crystalline pore wall was reported so far. Six phosphonate groups present in phytic acid helps extensive cross-linking to form and facilitate rapid gelation of the initial sol. Hydrothermal treatment of the gel and subsequent slow drying give rise to the final monolith and this has been shown by the digital images in Figure 1. In the

Figure 1. Photographs of gel formation (left) at (a) 1, (b) 3, and (c) 5 min and final monolith (right).

FTIR spectrum (see Figure S1 in the Supporting Information) of the material the sharp band centered around 1050 cm^{-1} is attributed to P−O−Sn stretching vibration.[7] The small bands in the range 2850−2930 cm^{-1} are assigned to C−H stretching vibrations of the phytic acid moiety. ^{31}P MAS NMR spectrum (see Figure S2a in the Supporting Information) of MLSnP-1 shows a clear and well-resolved signal centered at −12.5 ppm. This peak is characteristic of phosphorus atom with undissociated P−O−H group and the sharpness of the signal is related to uniform environment around P atoms and it indicates crystallinity of the material.[25] The ^{13}C MAS NMR signal (see Figure S2b in the Supporting Information) at around 75 ppm indicates presence of O-alkyl carbon in the material.[26] Atomic absorption spectrophotometric (AAS) and CHN elemental analyses show that the material contains 35.2% Sn, 7.1% C, and 2.7% H. From thermogravimetric analysis (TGA), shown in Figure S3 in the Supporting Information, a sharp ∼18% weight loss is observed in the temperature range of

590−720 K. It is possibly due to breakdown of the organic moiety and loss of carbon, hydrogen, and the bridging oxygen between carbon and phosphorus. From these thermal and elemental analysis data the material can be formulated as $C_6H_{12}P_6O_{24}Sn_3{\cdot}xH_2O$. Powder X-ray diffraction pattern (PXRD) (Figure 2a) of the material shows no peak in the small-angle region. This observation is common for some monolithic structures with disordered pore arrangement.[27] It was previously argued that monolithic mesoporous materials with microporosity in the pore wall might decrease scattering power and could lead to absence of small angle diffraction peak. Wide-angle PXRD pattern (Figure 2b) shows three distinct broad peaks centered at 2θ = 14.1 (6.3 Å), 30.5 (2.9 Å), and 42.1 (2.1 Å) and these indicate crystalline pore wall of the material. Crystallinity in this material originates from the periodic stacking and cross-linking of the multidentate phytic acid moieties connected to tin centers. This kind of periodic arrangement leading to crystalline pore wall is known from previous studies on organic−inorganic hybrid materials.[28]

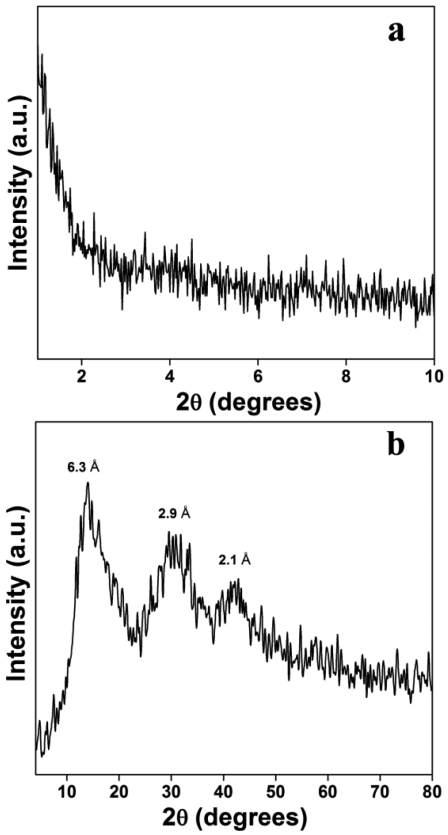

Figure 2. (a) Small-angle and (b) wide-angle powder X-ray diffraction patterns.

N_2 Adsorption Analysis. N_2 adsorption/desorption experiment of the material shows a "type IV-like" isotherm (Figure 3) with BET surface area of 347 m^2 g^{-1}. Although it resembles a type-I isotherm at very low P/P_o, considerable amount of multilayer adsorption has occurred in the relative pressure range of 0.02 to 0.4 and it indicates presence of mesoporosity in the material. Similar type of isotherm has been observed for small pore MCM-41 analogues,[29] mesoporous mixed oxides,[30] porous activated carbons,[31] where pore sizes are in the range of supermicroporous to small mesoporous region. The pore size distribution pattern (NLDFT) in the inset of Figure 3 shows

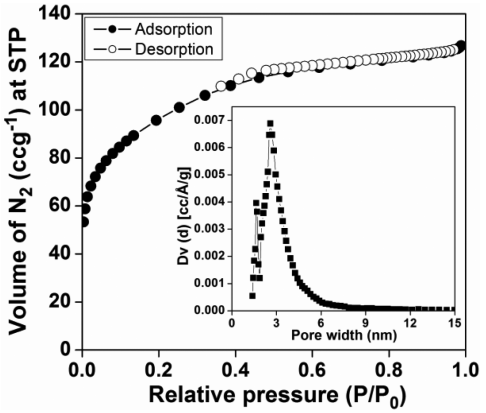

Figure 3. N_2 adsorption/desorption isotherm and pore size distribution (in the inset) of MLSnP-1. Error limit less than 1%.

that there is a sharp distinct peak and a small peak at 2.5 and 1.5 nm, respectively.

Microstructural Analysis. The scanning electron microscopic (SEM) images (Figure 4a and b) of the material reveal big particle morphology with various shapes. The surface architecture of the particles is quite smooth with sharp edges and these are consistent with crystalline feature of the material. From the transmission electron microscopic (TEM) image in Figure 4c it is seen that there are randomly oriented pores in the material as the disorder is also evidenced by the lack of small-angle diffraction peak in the PXRD pattern. The pore wall crystallinity and crystal fringes are visible from the high resolution TEM image in Figure 4d. The corresponding fast Fourier transform (FFT) image is also shown in the inset of Figure 3d.

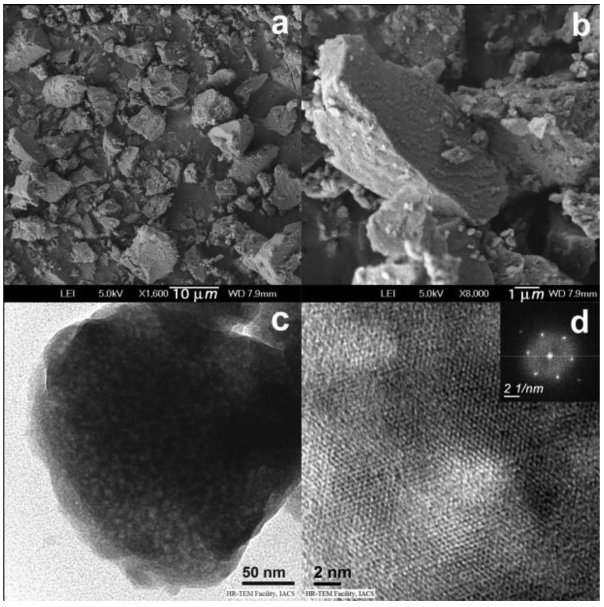

Figure 4. (a, b) SEM, (c) TEM, and (d) HR TEM images of MLSnP-1. The corresponding FFT pattern in shown in the inset of d.

Catalytic Study. The catalytic activity of the material was tested for esterification of long chain fatty acids with methanol. When the raw material for biodiesel synthesis contains high amount of FFA, they are easily saponified by the alkaline catalysts which are generally used during industrial production

dx.doi.org/10.1021/am402714r | ACS Appl. Mater. Interfaces 2013, 5, 9913−9917

and it complicates the synthesis as well as purification of the product. Usually, a two step process is performed to solve the problem. The first step is the acid catalyzed esterification of FFAs and the second step is the base catalyzed transesterification of triglycerides. One step conversion is also possible but by using hazardous catalysts such as H_2SO_4 at high temperature.[32] So, more and more active, green and ecofriendly acid catalysts for FFA esterification are very much desirable for successful and economical synthesis of biodiesel. Several different catalysts have been reported so far for the production of biodiesel.[33,34] Porous solid acid catalysts are also known to be efficient for this purpose.[35,36] But in most of the cases moderately high temperatures[37] are required and in few cases hazardous organic solvents are used[38] to carry out the reactions. Moreover, despite all these efforts, room temperature synthesis of biodiesel is very rarely reported.[39] Recently, our group have reported a hybrid porous sulfonated zinc phosphonate catalyst which is efficient for biodiesel synthesis at room temperature.[40] But sulfonation is an extra step for generating active catalytic center and it substantially reduces the surface area of the material. Here we have chosen different long chain aliphatic acids (CH_3-$(CH_2)_n$-COOH, n = 10, 12, 14, 16) as representatives of FFAs. Depending upon the chain length, 93−99% isolated yield of the corresponding ester was obtained within 6 h at 323 K over MLSnP-1. The catalytic reaction was so rapid that 70% yield of the ester was obtained at the reaction time of 2 h when lauric acid (n = 10) was used. Reaction kinetics for the esterification of lauric acid is shown in Figure 5.

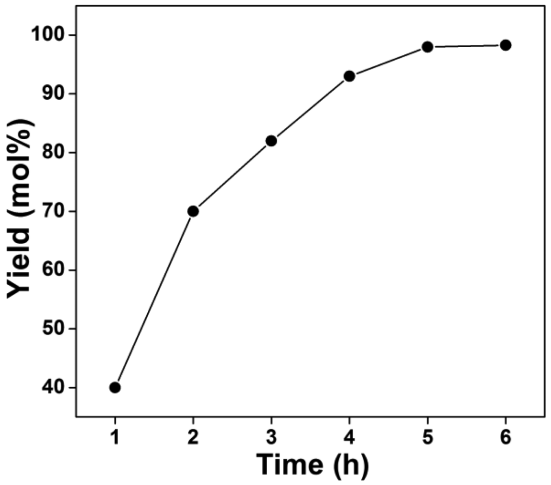

Figure 5. Reaction kinetics of esterification of lauric acid at 323 K. Error limit ±2%.

The catalytic activity of MLSnP-1 was also tested for unsaturated fatty acid and long chain dicarboxylic acid. For both the cases, good yield was obtained in short reaction time. Moreover for the dicarboxylic acid, only dimethyl ester was produced selectively.

The catalyst MLSnP-1 also showed excellent catalytic activity at room temperature and 94% isolated yield was obtained for lauric acid. The catalytic reactions in the present study are found to be much faster compared with many other catalysts including homogeneous and heterogeneous tin based catalysts.[23] In addition to these, tin-based materials need various modifications to generate the active sites in the catalysts.[41,42] But we have used the as-made air-dried monolithic material for catalytic reactions. In all the reactions described above, we used excess of methanol that acted as a solvent besides taking part in the esterification reaction. We were also interested to verify the catalytic activity under equal amount (w/w) of acid and methanol for this reaction. The yield of the product was 88% in 10 h when lauric acid was used as a representative fatty acid. When the same reaction was carried out at room temperature, yield was 81% in 24 h of reaction time. The catalyst was recycled for five times without any significant loss of catalytic activity and it has been shown in Figure 6.

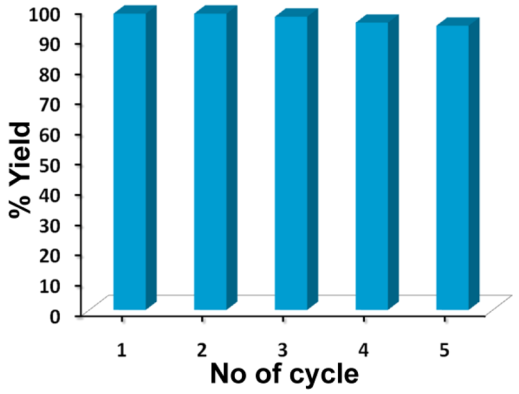

Figure 6. Recycling efficiency of MLSnP-1 catalyst. Error limit ±2%.

Table 1. Esterification of Different Fatty Acids by MLSnP-1 Catalyst

acid	acid:MeOH:Sn	time (h)	temperature (K)	Yield[a] (%)
lauric acid	1:120:0.08	5	323	99
myristic acid	1:120:0.08	5	323	98
palmitic acid	1:120:0.08	6	323	98
stearic acid	1:120:0.08	6	323	93
oleic acid	1:120:0.08	5	323	94
sebacic acid	1:120:0.08	6	323	85
lauric acid	1:120:0.08	15	298	94
lauric acid	1:6:0.08	10	323	88
lauric acid	1:6:0.08	24	298	81
oleic acid[b]	1:120:0	24	323	9
oleic acid[b]	1:120:0	24	298	5
lauric acid[c]		10	323	31

[a]Isolated and purified yield (error limit ±2%). [b]Without catalyst.[34] [c]Phytic acid (0.1 mmol) as homogeneous catalyst.

When the reaction was carried out in the absence of MLSnP-1 catalyst, yield of the esterification products was very poor (5−9%). Phytic acid was also used as catalyst for comparison. Yield was much less compared to MLSnP-1 catalyst using lauric acid as FFA. Most serious drawback of using phytic acid as catalyst is that it forms homogeneous phase with the reactant. Thus, it is not comparable with heterogeneous catalyst MLSnP-1, which showed excellent recyclability. When transesterification reaction of ethyl cyanoacetate was carried out in methanol, MLSnP-1 catalyst did not show any significant activity. No detectable amount of methyl ester was formed after 10 h of reaction at 323 K. Very little amount of product was obtained only after continuing the reaction up to 24 h. We have also carried out leaching test to confirm true heterogeneity of the reaction and esterification of lauric acid was taken as the representative reaction. The catalyst was separated after 2 h and the reaction was continued up to 6 h. The yield of the product was found to be 76% at 6 h vis-à-vis 70% yield at 2 h. The reaction mixture

was also analyzed by AAS and no detectable amount of tin was found. Surface Lewis acidity of the material was tested by pyridine adsorption on the surface and monitoring the desorption of loosely bound pyridine molecules by temperature programmed FTIR spectra (see Figure S4 in the Supporting Information). At low temperature, there is a peak observable around 1400 cm^{-1} for the adsorbed pyridine molecules at the surface of the material. With the increase in temperature, the peak intensity diminishes because of desorption of pyridine.

CONCLUSION

A new monolithic mesoporous tin(IV) phosphonate material with crystalline pore wall has been synthesized by template free sol–gel route. Phytic acid was used as the phosphonate source and tin(IV) chloride was used as the inorganic precursor. Gel formation was found to be very rapid and hydrothermal treatment of initially formed gel followed by slow drying gave the monolithic structure. This material showed excellent catalytic activity for esterification of long chain fatty acids with methanol at room temperature. Although the catalytic activity of this monolithic catalyst has been tested at liquid phase under stirring conditions, we believe the monolithic property of the material can be utilized for other applications, especially under fixed bed conditions in the future.

ASSOCIATED CONTENT

Supporting Information

^{1}H and ^{13}C NMR data, FTIR and solid-state MAS NMR spectra, thermal analysis data and temperature programmed pyridine desorption IR spectra are provided in this section. This material is available free of charge via the Internet at http://pubs.acs.org.

AUTHOR INFORMATION

Corresponding Author

*E-mail: msab@iacs.res.in.

Notes

The authors declare no competing financial interest.

ACKNOWLEDGMENTS

A.D. and A.K.P. thank CSIR, New Delhi, for their senior research fellowships. A.B. thanks DST New Delhi for providing instrumental facility through the DST Unit on Nanoscience.

REFERENCES

(1) Horike, S.; Dinca, M.; Tamaki, K.; Long, J. R. *J. Am. Chem. Soc.* **2008**, *130*, 5854–5855.
(2) Mal, N. K.; Fujiwara, M.; Tanaka, Y. *Nature* **2003**, *421*, 350–353.
(3) Ren, S.; Chang, L.-Y.; Lim, S.-K.; Zhao, J.; Smith, M.; Zhao, N.; Bulović, V.; Bawendi, M.; Gradecak, S. *Nano Lett.* **2011**, *11*, 3998–4002.
(4) Chang, C.-C.; Chen, W.-C. *Chem. Mater.* **2002**, *14*, 4242–4248.
(5) Dutta, A.; Nandi, M.; Sasidharan, M.; Bhaumik, A. *ChemPhysChem* **2012**, *13*, 3218–3222.
(6) Dutta, A.; Mondal, J.; Patra, A. K.; Bhaumik, A. *Chem.—Eur. J.* **2012**, *18*, 13372–13378.
(7) Dutta, A.; Pramanik, M.; Patra, A. K.; Nandi, M.; Uyama, H.; Bhaumik, A. *Chem. Commun.* **2012**, *48*, 6738–6740.
(8) Dutta, A.; Patra, A. K.; Bhaumik, A. *Microporous Mesoporous Mater.* **2012**, *155*, 208–214.
(9) Cabrera, K. *J. Sep. Sci.* **2004**, *27*, 843–852.
(10) Legido-Quigley, C.; Marlin, N. D.; Melin, V.; Manz, A.; Smith, N. W. *Electrophoresis* **2003**, *24*, 917–944.
(11) Drisko, G. L.; Zelcer, A.; Wang, X. D.; Caruso, R. A.; Soler-Illia, G. J. de A. A. *ACS Appl. Mater. Interfaces* **2012**, *4*, 4123–4130.
(12) Kanamori, K.; Nakanishi, K. *Chem. Soc. Rev.* **2011**, *40*, 754–770.
(13) Peters, E. C.; Svec, F.; Fréchet, J. M. J. *Adv. Mater.* **1999**, *11*, 1169–1181.
(14) Haughton, L.; M. J. Williams, J. *J. Chem. Soc., Perkin Trans. 1* **1999**, 2645–2658.
(15) Zhang, H.; Hardy, G. C.; Khimyak, Y. Z.; Rosseinsky, M. J.; Cooper, A. I. *Chem. Mater.* **2004**, *16*, 4245–4256.
(16) Kido, Y.; Nakanishi, K.; Miyasaka, A.; Kanamori, K. *Chem. Mater.* **2012**, *24*, 2071–2077.
(17) Ma, T.-Y.; Yuan, Z.-Y. *Chem. Commun.* **2010**, *46*, 2325–2327.
(18) Ohtani, B.; Ogawa, Y.; Nishimoto, S.-i. *J. Phys. Chem. B* **1997**, *101*, 3746–3752.
(19) Smatt, J.-H.; Spliethoff, B.; Rosenholm, J. B.; Linden, M. *Chem. Commun.* **2004**, 2188–2189.
(20) Kirumakki, S.; Huang, J.; Subbiah, A.; Yao, J.; Rowland, A.; Smith, B.; Mukherjee, A.; Samarajeewa, S.; Clearfield, A. *J. Mater. Chem.* **2009**, *19*, 2593–2603.
(21) Kirumakki, S.; Samarajeewa, S.; Harwell, R.; Mukherjee, A.; Herber, R. H.; Clearfield, A. *Chem. Commun.* **2008**, 5556–5558.
(22) Subbiah, A.; Pyle, D.; Rowland, A.; Huang, J.; Narayanan, R. A.; Thiyagarajan, P.; Zoń, J.; Clearfield, A. *J. Am. Chem. Soc.* **2005**, *127*, 10826–10827.
(23) Cardoso, A. L.; Neves, S. C. G.; da Silva, M. J. *Energy Fuels* **2009**, *23*, 1718–1722.
(24) Pramanik, M.; Nandi, M.; Uyama, H.; Bhaumik, A. *Catal. Sci. Technol.* **2012**, *2*, 613–620.
(25) Hudson, M. J.; Workman, A. D. *J. Mater. Chem.* **1991**, *1*, 375–379.
(26) Norris, C. E.; Quideau, S. A.; Landhausser, S. M.; Bernard, G. M.; Wasylishen, R. E., *Sci. Rep.* 2012, *2*.
(27) Smått, J.-H.; Schunk, S.; Lindén, M. *Chem. Mater.* **2003**, *15*, 2354–2361.
(28) Inagaki, S.; Guan, S.; Ohsuna, T.; Terasaki, O. *Nature* **2002**, *416*, 304–307.
(29) Schmidt, R.; Stöcker, M.; Hansen, E.; Akporiaye, D.; Ellestad, O. H. *Microporous Mater.* **1995**, *3*, 443–448.
(30) Patra, A. K.; Dutta, A.; Bhaumik, A. *ACS Appl. Mater. Interfaces* **2012**, *4*, 5022–5028.
(31) Kaneko, K.; Ishii, C.; Ruike, M.; kuwabara, H. *Carbon* **1992**, *30*, 1075–1088.
(32) Vasudevan, P. T.; Briggs, M. *J. Ind. Microbiol. Biotechnol.* **2008**, *35*, 421–430.
(33) Stöveken, T.; Steinbüchel, A. *Angew. Chem., Int. Ed.* **2008**, *47*, 3688–3694.
(34) Gang, L.; Xinzong, L.; Eli, W. *New J. Chem.* **2007**, *31*, 348–351.
(35) Das, S. K.; Bhunia, M. K.; Sinha, A. K.; Bhaumik, A. *ACS Catal.* **2011**, *1*, 493–501.
(36) Pirez, C.; Caderon, J. M.; Dacquin, J. P.; Lee, A. F.; Wilson, K. *ACS Catal.* **2012**, *2*, 1607–1614.
(37) Dhainaut, J.; Dacquin, J.-P.; Lee, A. F.; Wilson, K. *Green Chem.* **2010**, *12*, 296–303.
(38) Zabeti, M.; Wan Daud, W. M. A.; Aroua, M. K. *Fuel Process. Technol.* **2009**, *90*, 770–777.
(39) Chintareddy, V. R.; Ho, H.-A.; Sadow, A. D.; Verkade, J. G. *Tetrahedron Lett.* **2011**, *52*, 6523–6529.
(40) Pramanik, M.; Nandi, M.; Uyama, H.; Bhaumik, A. *Green Chem.* **2012**, *14*, 2273–2281.
(41) Moreno, J. I.; Jaimes, R.; Gómez, R.; Niño-Gómez, M. E. *Catal. Today* **2011**, *172*, 34–40.
(42) Sarkar, A.; Ghosh, S. K.; Pramanik, P. *J. Mol. Catal. A: Chem.* **2010**, *327*, 73–79.